Osmotic Flow through Fully Permeable Nanochannels

C. Lee,[1,2] C. Cottin-Bizonne,[1] A.-L. Biance,[1] P. Joseph,[3,4] L. Bocquet,[1,*] and C. Ybert[1,†]
[1]Institut Lumière Matière, Université Claude Bernard Lyon 1-CNRS, UMR 5306, Université de Lyon, F-69622 Villeurbanne Cedex, France
[2]School of Aerospace and Mechanical Engineering, Korea Aerospace University, Goyang 412-791, Korea
[3]CNRS, LAAS, 7 Avenue du Colonel Roche, F-31400 Toulouse, France
[4]Université de Toulouse, LAAS, F-31400 Toulouse, France
(Received 28 February 2014; published 19 June 2014)

Osmosis across membranes is intrinsically associated with the concept of semipermeability. Here, however, we demonstrate that osmotic flow can be generated by solute gradients across nonselective, fully permeable nanochannels. Using a fluorescence imaging technique, we are able to measure the water flow rate inside single nanochannels to an unprecedented sensitivity of femtoliters per minute flow rates. Our results indicate the onset of a convective liquid motion under salinity gradients, from the higher to lower electrolyte concentration, which is attributed to diffusio-osmotic transport. To our knowledge, this is the first experimental evidence and quantitative investigation of this subtle interfacially driven transport, which need to be accounted for in nanoscale dynamics. Finally, diffusio-osmotic transport under a neutral polymer gradient is also demonstrated. The experiments highlight the entropic depletion of polymers that occurs at the nanochannel surface, resulting in convective flow in the opposite direction to that seen for electrolytes.

DOI: 10.1103/PhysRevLett.112.244501 PACS numbers: 47.61.Fg, 82.39.Wj, 47.57.jd

Osmotic transport plays a crucial role in many areas of science and technology, from transport across biological membranes in living matter, to technological applications in desalination process using, e.g., reverse osmosis, food processing, or energy harvesting under salinity gradients [1–5]. When two reservoirs with different solute concentrations are put into contact via a semipermeable membrane —i.e., a membrane that is impermeable to the solute, while allowing free passage of water—an osmotic pressure drop builds up between the two sides and a corresponding water flux is initiated in order to reach thermodynamic equilibrium. For low solute concentration, the osmotic pressure drop is given by the famous van't Hoff formula in the form of a perfect gas expression $\Delta\Pi = k_B T \Delta C_{\mathrm{sol}}$, with ΔC_{sol} the solute concentration difference across the membrane [1]. For a $1M$ salinity contrast, $\Delta\Pi \sim 50$ bar and the effects of osmosis are of considerable importance.

However, there are, in principle, alternative ways to take benefit from salinity gradients and osmotic response, beyond the canonical semipermeable membrane geometry. As was pointed out by Derjaguin and first explored by Derjaguin [6], and Anderson, Prieve, and coworkers [7,8], an interfacially driven version of osmotic transport may be achieved under salinity gradients in the presence of a solid surface. For particles, this leads to a (diffusio)phoretic migration, which can be used to manipulate colloids and macromolecules under tunable solute gradients [8–14].

Physically, this originates in a (diffusio-)osmotic flow driven by an osmotic pressure gradient that builds up within the diffuse layer at the solid surface. Such diffusio-osmotic transport [15] was recently suggested to account for the strongly increased rate of translocation of DNA through a nanopore in the presence of a salt gradient [16]. In a different energy-harvesting context, diffusio-osmosis was also proposed to be at the origin of a very large electric current generation under salinity gradients inside boron nitride nanotubes [4]. As an interesting, but counterintuitive, property, diffusio-osmosis should operate across a membrane without the requirement of solute rejection. This opens various perspectives in terms of applications by relaxing some of the constraints on the nanoscale semipermeable membranes.

Despite this growing interest and significance in nanodevices, there remains a strong need to investigate further, from an experimental point of view, the detailed origin of this subtle phenomenon, which originates in the force balance within the first few nanometers close to surfaces. Indeed, so far no direct experimental evidence of the generation of flow through diffusio-osmosis has been reported, while existing studies have essentially explored either indirect manifestations of this phenomenon on electrical transport or its counterpart for particle transport, as discussed above.

In the present study, we experimentally demonstrate for the first time a diffusio-osmotic flow generation, by investigating the liquid transport properties along nanochannels submitted to a gradient of solutes. Using a fluorescence imaging technique, we evidence the onset of a water flow under solute gradients, achieving an unprecedented flow rate sensitivity. Both transport under salinity gradients and polymer gradients are explored, which allows us to gain much insight into the origin of this transport phenomenon.

The micro-nanodevices are fabricated using Si chips by conventional nanofabrication techniques with nanochannels bridging between two side microchannels [Fig. 1(a)] [17]. The nanochannels are $h = 163$ nm in height, $w = 5$ μm wide, and $L = 150$ μm long. The surface was electrically insulated with a 100 nm thick silicon oxide layer grown by thermal oxidation, and then a silicon wafer was anodically bonded onto a 170 μm thick Pyrex glass wafer. For practical purposes, an array of 17 parallel nanochannels is etched on each device, but experiments are all performed at the single nanochannel level, in different chips and nanochannels. In the following, all solute solutions consist of various concentrations of added salts (KI, NaI, or LiI) in a background Tris solution (1 mM Tris-HCl, 2 mM NaOH), except in Fig. 4, where a neutral polymer (PEG-200) is used as solute. Well-controlled solute concentration boundary conditions at nanochannel ends are obtained by circulating the left (right) microchannel arm with a solution of solute concentration n_L (n_R) prior to microchannel insulation in order to minimize spurious residual convection.

As a probe for a generated water flow, we use a fluorescent molecular dye ($C_f^0 = 200$ μM fluorescein salt) in the left microchannel only, and record the fluorescence intensity signal using confocal microscopy (Leica TCS SP5). We checked independently that in the present conditions, the fluorescence intensity is indeed proportional to the probe concentration $C_f(x)$. Typical results for the intensity profile are shown in Figs. 1(b)–1(c): while under pure diffusion the fluorescence intensity profile along a nanochannel would be expected to be linear in space, we measure a strong deviation from the linear behavior whenever a solute gradient is imposed between the two ends of the nanochannel. Furthermore, this deviation from linearity is found to depend on the sign and amplitude of the solute gradient [compare Figs. 1(b) and 1(c)].

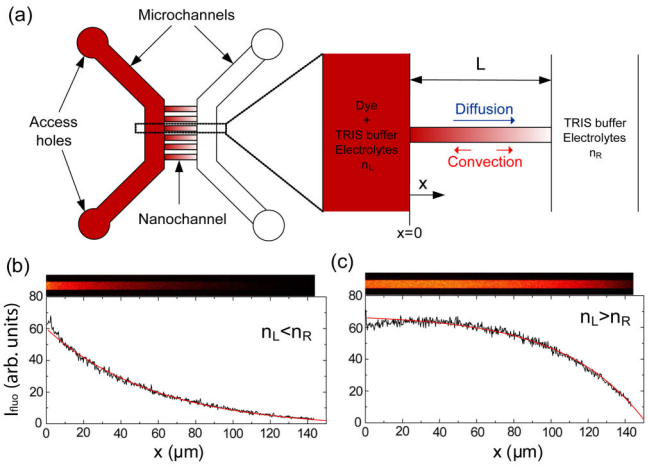

FIG. 1 (color online). (a) Device layout. Nanochannels ($h = 163$ nm, width $w = 5$ μm, length $L = 150$ μm) bridge between two microchannels, with 300×50 μm^2 cross section, in which solutions of different solute concentrations [n_L (n_R) in the left (right) arm] can be circulated to control the solute gradient along nanochannels. (b),(c) Steady state fluorescent probe intensity profiles along nanochannels for different solute (NaI) imbalances (b) $n_L < n_R$ (1 and 30 mM) and (c) $n_R < n_L$ (30 and 1 mM). Solid line (red): fit according to diffusion-convection equations (1); all profiles are seen to strongly depart from the linear diffusive-only theoretical profile.

This deviation is the experimental signature of an additional convective drift of the fluorescent probe. In the presence of a flow rate $\tilde{Q}$, the steady-state concentration of the probe, $C_f(x)$, obeys the stationary diffusion-convection equation

$$\frac{\tilde{Q}}{wh}\partial_x C_f = D_f \partial_x^2 C_f, \tag{1}$$

with D_f the diffusivity of the fluorescent dye ($D_f = 3.5 \times 10^{-10}$ m^2/s for fluorescein [18]); only the dependence along the channel length x is studied. The probe profile C_f is predicted to take the form of an exponentially decaying function. Comparison to experimental data is shown in Figs. 1(b)–1(c), yielding a very good agreement with the predicted profiles. This allows us to extract the only unknown, $\tilde{Q}$, with a sensitivity of about 50 fl/min. As a comparison, this is 2 to 3 orders of magnitude smaller than what was recently measured by a state-of-the-art technique (10 pl/min) in a similar nanochannel geometry [19].

Going beyond this first observation, we have systematically investigated the evolution of the flow rate $\tilde{Q}$ with different salt nature (KI, NaI, and LiI) and concentration imbalance between nanochannel ends. Figure 2 shows the measured $\tilde{Q}$, as a function of the raw added-salt concentration difference $n_R - n_L$ (Fig. 2, inset) or, as we shall explain in the following, as a function of the difference in

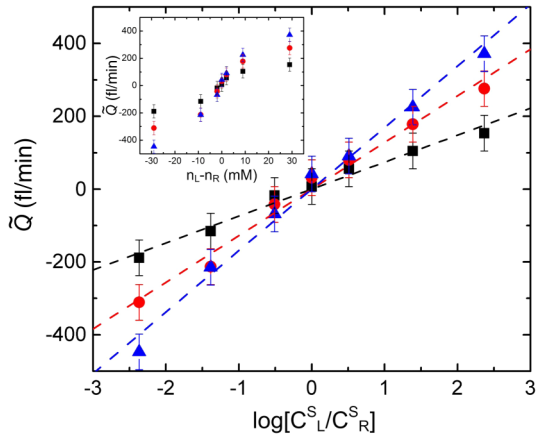

FIG. 2 (color online). Measured flow rate $\tilde{Q}$ as a function of the difference between logarithmic electrolyte concentrations C^s (see text) for three different added salts: (■) KI, (•) NaI, (▲) LiI. Inset: same data with flow rate plotted against added-salt concentration difference $n_L - n_R$.

logarithmic electrolyte concentration (Fig. 2). Overall, we observe at first glance that for all salts there exists a flow rate oriented from high to low concentrations, with a magnitude that increases with the concentration difference. We additionally observe a salt-specific effect with convective transport increasing following the order KI < NaI < LiI.

More fundamentally, this experiment suggests the onset of osmotically generated convective transport, and hence liquid flow, under salt gradients. However, we emphasize that in the present conditions, the nanochannels are fully permeable to the salt. Indeed, the Debye length λ_D that characterizes the extent of wall-solute electrostatic interaction in the system is expected to be always below 10 nm so that no salt exclusion occurs ($\lambda_D \ll h$). This result contrasts strongly with the common description of osmotic flows where solute rejection is a prerequisite to express the osmotic pressure.

As we now show, this unexpected result originates in diffusio-osmosis (DO), an interfacially driven transport mechanism belonging to the same class of transport phenomena as electro-osmosis or thermo-osmosis. When submitted to a longitudinal electrolyte concentration gradient, it is theoretically predicted that a plug velocity is generated in the channel in the presence of a charged solid surface. This wall-induced velocity takes the form [7]

$$u_{\mathrm{slip}}(x) = -D_{\mathrm{DO}} \nabla \log(C^s) \tag{2}$$

with D_{DO} the diffusio-osmotic mobility and C^s the electrolyte concentration, which for a moderate buffer reads as the sum of added-salt (KI, NaI, LiI) and homogeneous background concentrations $C^s(x) \simeq n(x) + c_{\mathrm{bkg}}$. Now, in the presence of a linear gradient of solute, the logarithmic dependence of u_{slip} in Eq. (2) generates a finite pressure gradient. The flow within the nanochannel thus reads as the superimposition of the diffusio-osmotic plug flow and a Poiseuille contribution, $Q = wh(u_{\mathrm{slip}} - ((h^2 \nabla P)/12\eta))$, with η the liquid viscosity. Integrating the constant flow rate Q along the nanochannel, with the boundary condition $P_R - P_L = 0$, eventually yields

$$Q = \frac{wh}{L} \int u_{\mathrm{slip}}(x) dx = \frac{wh}{L} D_{\mathrm{DO}} \log\left(\frac{C_L^s}{C_R^s}\right). \tag{3}$$

This predicts a logarithmic dependency of the flow rate with the ratio C_L^s/C_R^s. This prediction appears in very good agreement with the experimental results reported in Fig. 2, where the measured flow rate $\tilde{Q}$ is found to behave linearly with $\log(C_L^s/C_R^s)$, in agreement with Eq. (3).

To go further in the quantitative analysis requires entering into more details in the description of both the theoretical modeling of (diffusio-)osmotic effects [7,8,20] and the experimental configuration. Indeed, for electrolytes as solutes, it was predicted that the diffusio-osmotic response D_{DO} can be split into two contributions [7],

$$D_{\mathrm{DO}} = K_{\mathrm{CO}} - \beta K_{\mathrm{EO}}. \tag{4}$$

The first term K_{CO} is a truly osmotic contribution, referred to as the chemiosmotic effect, which arises due to the excess osmotic pressure gradients existing along the surface within the nanometric Debye layer. Within the Poisson-Boltzmann framework for ion-surface interactions, this terms takes the expression

$$K_{\mathrm{CO}} = \frac{k_B T}{\eta} \frac{[-\log(1-\gamma^2)]}{2\pi \ell_b}, \tag{5}$$

with $\gamma = \tanh(\phi/4)$, $\phi = (eV_s/k_BT)$, e the elementary charge, V_s the surface potential, ℓ_b the Bjerrum length, k_B the Boltzmann constant, and T the temperature (here 290 K) [7,21].

The second contribution, $-\beta K_{\mathrm{EO}}$, takes its origin in the electro-osmotic response of the surface, induced by a diffusion-induced tangential electric field [22]. The latter stems from the difference in anion and cation diffusivities D_+ and D_- [7,23] and reads $E \simeq \beta(k_BT/e)\nabla \log C^s$, where $\beta = (D_+ - D_-)/(D_+ + D_-)$ [7,10]. With a classical electro-osmotic mobility given by $-\varepsilon\zeta/\eta$ [21], where ε is the liquid permittivity and ζ the surface zeta potential, this predicts [7]

$$K_{\mathrm{EO}} = -\frac{e\zeta}{4\pi\eta\ell_B}. \tag{6}$$

Experimentally the liquid flow is probed through the convective transport of a fluorescent dye. Because fluorescein is a dianion at basic pH, it does not behave as a passive tracer and experiences an additional electrophoretic drift under electric field, characterized by its mobility μ_{EP} ($\mu_{\mathrm{EP}} \simeq -2.8 \times 10^{-8}$ m^2 V^{-1} s^{-1}). Note that neutral dye would overcome this complication, but we found that this induced several experimental issues with adsorption inside the nanochannel and an associated spurious signal compromising the intensity-concentration conversion.

Overall, we expect the molecular dye flow rate $\tilde{Q}$ to obey the same equation Eq. (3) as the solvent flow rate Q, but with a modified response coefficient,

$$\tilde{D}_{\mathrm{DO}} = K_{\mathrm{CO}} - \beta(K_{\mathrm{EO}} + zD_f), \tag{7}$$

where $D_f = k_BT\mu_{\mathrm{EP}}/ze$, with $z = -2$ the fluorescein valency.

Beyond the linearity in $\log(C_L^s/C_R^s)$, this theoretical prediction captures the salt-specific effect evidenced in Fig. 2. Indeed, the three studied electrolytes KI, NaI, LiI are characterized by decreasing cation diffusivities [24], so that the amplitudes of the osmotic flow are ordered following the increasing $|\beta|$ coefficients: KI < NaI < LiI. More quantitatively, Eqs. (3)–(7) allow us to extract the diffusio-osmotic mobility D_{DO} for each salt from the slope measurement in Fig. 2. In Fig. 3 we then plot D_{DO} versus

the coefficient $-\beta$, which confirms the expected linear behavior. Moreover, the intercept and slope measurements in Fig. 3 allow us to extract, respectively, the chemiosmotic K_{CO} and electro-osmotic K_{EO} contributions to the solvent flow, yielding $V_s = -55 \pm 4$ mV and $\zeta = -98 \pm 10$ mV for the surface properties. Such values agree with the electrical properties of silica surfaces in comparable electrolyte concentrations as found in the literature [25].

Now to complement the diffusio-osmotic experiments, it is also possible to carry on an independent measurement of the ζ potential through investigations of the electro-osmotic velocity under an externally applied voltage difference across the very same system. Ag/AgCl electrodes were used to impose the electric potential in reservoirs. Note that to account for the chip geometry, the actual electric field within the nanochannel was calculated according to the equivalent resistance pattern as $E = (\Delta V/L)(R_{\text{nano}}/[R_{\text{nano}} + R_{\text{micro}}])$. There, electric resistances read $R_{\text{micro}} = L_{\text{micro}}/(\sigma h_{\text{micro}} w_{\text{micro}})$ and $R_{\text{nano}} = L_{\text{nano}}/(N\sigma h_{\text{nano}} w_{\text{nano}})$ with σ the bulk electrolyte conductivity and N the number of parallel nanochannels on the chip. In the following, an intermediate salt concentration of 10 mM was used; accordingly, corrections for the surface conductivity can be safely ignored in our $h = 163$ nm thick nanochannels [26,27]. We then make use of the same measurement method as described above to measure the electro-osmotic liquid velocity. The latter is compared to the theoretical relationship—accounting for dye electrophoresis—as given by

$$\tilde{Q} = \frac{wh}{L}\left(\mu_{\text{EP}} - \frac{\varepsilon\zeta}{\eta}\right)E. \tag{8}$$

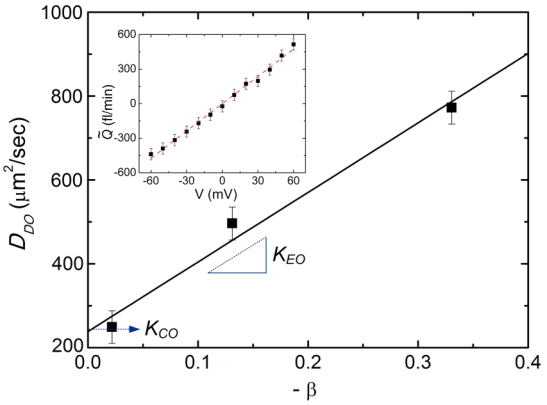

FIG. 3 (color online). Dependence of diffusio-osmotic mobility D_{DO} as a function of the mobility mismatch coefficient $-\beta$: (■) data point from Fig. 2 (see text), (solid line) linear fit. Inset: electro-osmotic characterization of nanochannel surfaces showing measured dye flow rate $\tilde{Q}$ as a function of imposed electric potential difference. (■) data points, (dashed line) best fit according to Eq. (8) yielding $\zeta = -85 \pm 2$ mV.

The measured dye convective flow rate is plotted against applied voltage difference in the inset of Fig. 3. The linear dependency is well recovered from which the nanochannel surface zeta potential can be extracted, yielding $\zeta = -85 \pm 2$ mV. This is fully consistent with the zeta potential obtained from K_{EO} and more generally with the surface characteristics deduced from osmotically generated flows. Note that the differences found in V_s and ζ are reminiscent of classically observed variations between electrokinetic phenomena probing either the surface charge (chemiosmosis) or the zeta potential (electro-osmosis) [21].

Finally, going beyond electrolytes as a solute, we now turn to diffusio-osmotic transport using gradients of a neutral species, here a low molecular polyethylene glycol (PEG) polymer (MW 200 g/mol). Polymers constitutes the prototypical solute in standard membrane osmosis, where effects arise from size exclusion from the pores (e.g., in routine solution dialysis). However it must be stressed that no such exclusion exists here with a polymer gyration radius of $R_G \simeq 0.4$ nm [28]. This value of R_G is orders of magnitudes smaller than the nanochannel height h (163 nm in the present case) and, hence, based on the standard osmotic picture across membranes, no effect should *a priori* be expected in this fully permeable channel.

On the contrary, we found experimentally in Fig. 4 that the PEG gradient along the nanochannel still leads to a water flow, in an analogous way to the electrolyte case. Unlike electrolytes, however, the dependency of the flow rate on solute gradient is linear while, as discussed above, it is found to be proportional to the gradient of the logarithm of the salt concentration. It thus reads

$$Q = \frac{wh}{L}\mu_{\text{DO}}[n_L - n_R] \tag{9}$$

with μ_{DO} a diffusio-osmotic mobility associated with PEG gradients and $n_L - n_R$ the polymer concentration difference

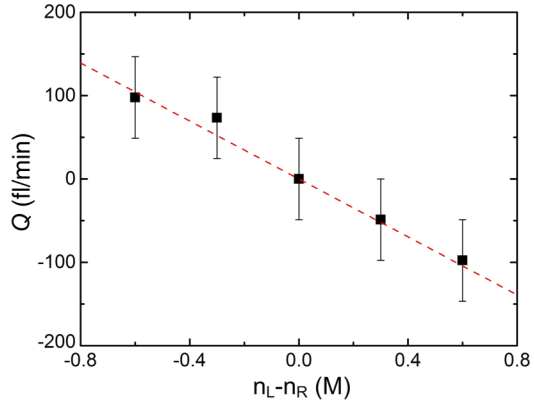

FIG. 4 (color online). Water flow rate as a function of the difference between neutral polymer concentrations n_L and n_R: (■) PEG (MW 200), (dashed line) linear fit yielding a slope of -173.5 ± 25 fl/min/M.

between nanochannel ends. Beyond the concentration dependency, a second major difference with the case of electrolytes is that the polymer-induced flow is found to go in the opposite direction, with the water flow driven towards the higher PEG concentration. This negative "chemotaxis" is consistent with a depleted polymer layer at the nanochannel surfaces [7]. Going further, if one assumes a steric (entropic) exclusion of the PEG from the walls with an exclusion region of extension R_G, the gyration radius of the PEG, the DO mobility is then predicted to behave as $\mu_{\mathrm{DO}} \sim -(k_B/\eta)R_G^2$. Using experimental data from Fig. 4 together with Eq. (9), one extracts a value $R_G^{\mathrm{expt}} = 0.47 \pm 0.04$ nm, to compare with expected polymer radius $R_G \simeq 0.4$ nm [28]. Both values do agree quantitatively, showing that the diffusio-osmosis probes in a very sensitive way the polymer-wall interface. This constitutes the first measurement of osmotic surface-driven transport with polymers, a phenomenon recently put forward as of central importance in the separation of biomolecules [13,14].

In this Letter we measured for the first time the diffusio-osmotic transport of a liquid induced by a concentration gradient of solutes. To this end, we have developed a fluorescence imaging technique allowing us to probe convective flow inside nanochannels with unprecedented sensitivity, reaching 50 fl/ min. In the case of an electrolyte as a solute, a diffusio-osmotic water flow is built under a salinity gradient from the higher to the lower salt concentration. Our experiments could disentangle the complementing effects of chemiosmosis and electro-osmosis, whose respective contributions to diffusio-osmosis were quantitatively evaluated. A similar diffusio-osmotic flow is demonstrated under concentration gradients of a neutral PEG, displaying, however, a reverse flow and pointing to a depletion of the polymer at the channel surface. This analysis clearly demonstrates that diffusio-osmosis allows us to induce osmotic transport without the constraints of solute rejection. Altogether diffusio-osmosis appears as a versatile and very efficient transport phenomenon that can play a significant role in the current development of nanodevices.

This research was supported by the ERC AG program, project Micromegas. We thank R. Fulcrand for help in fabricating the nanochannels. We thank LAAS and INL for access to their clean room facilities.

*Present address: Department of Civil and Environmental Engineering, Massachusetts Institute of Technology, Cambridge, MA, USA.
†Christophe.Ybert@univ-lyon1.fr

[1] O. Kedem and A. Katchalsky, J. Gen. Physiol. **45** 143 (1961).
[2] P. Sheeler and D. E. Bianchi, *Cell and Molecular Biology* (Wiley, New York, 1987).
[3] B. E. Logan and M. Elimelech, Nature (London) **488**, 313 (2012).
[4] A. Siria, P. Poncharal, A.-L. Biance, R. Fulcrand, X. Blase, S. Purcell, and L. Bocquet, Nature (London) **494**, 455 (2013).
[5] M. Elimelech and W. A. Phillip, Science **333**, 712 (2011).
[6] B. V. Derjaguin, S. S. Dukhin, and M. M. Koptelova, J. Colloid Interface Sci. **38**, 584 (1972).
[7] J. L. Anderson, Annu. Rev. Fluid Mech. **21**, 61 (1989).
[8] J. P. Ebel, J. L. Anderson, and D. C. Prieve, Langmuir **4**, 396 (1988).
[9] P. O. Staffeld and J. A. Quinn, J. Colloid Interface Sci. **130**, 88 (1989); **130**88 (1989).
[10] B. Abecassis, C. Cottin-Bizonne, C. Ybert, A. Ajdari, and L. Bocquet, Nat. Mater. **7**, 785 (2008).
[11] J. Palacci, B. Abecassis, C. Cottin-Bizonne, C. Ybert, and L. Bocquet, Phys. Rev. Lett. **104**, 138302 (2010).
[12] J. Palacci, C. Cottin-Bizonne, C. Ybert, and L. Bocquet, Soft Matter **8**, 980 (2012).
[13] Y. T. Maeda, A. Buguin, and A. Libchaber, Phys. Rev. Lett. **107**, 038301 (2011).
[14] H.-R. Jiang, H. Wada, N. Yoshinaga, and M. Sano, Phys. Rev. Lett. **102**, 208301 (2009).
[15] M. M. Hatlo, D. Panja, and R. van Roij, Phys. Rev. Lett. **107**, 068101 (2011).
[16] M. Wanunu, W. Morrison, Y. Rabin, A. Y. Grosberg, and A. Meller, Nat. Nanotechnol. **5**, 160 (2010).
[17] F. Chauvet, S. Geoffroy, A. Hamoumi, M. Prat, and P. Joseph,, Soft Matter **8**, 10738 (2012).
[18] D. Milanova, R. D. Chambers, S. S. Bahga, and J. G. Santiago, Electrophoresis **32**, 3286 (2011).
[19] K. Mathwig, D. Mampallil, S. Kang, and S. G. Lemay, Phys. Rev. Lett. **109**, 118302 (2012).
[20] Y. Mori, C. Liu, and R. S. Eisenberg, Physica (Amsterdam) **240D**, 1835 (2011).
[21] R. J. Hunter, *Foundations of Colloid Science* (Oxford University Press, New York, 1991).
[22] Note that a very similar effect exists under a thermal gradient, with the electric field arising there from differential anion and cation Soret coefficients [29].
[23] M. S. Munson, C. R. Cabrera, and P. Yager, Electrophoresis **23**, 2642 (2002).
[24] $D_+ = 1.957, 1.571, 1.029 \times 10^{-9}$ m^2/s for K^+, Na^+, Li^+, and $D_- = 2.045 \times 10^{-9}$ m^2/s for I^-. Let us stress that the salt specificity here at stake is therefore different from the one arising from specific interactions associated with the celebrated Hofmeister series.
[25] B. J. Kirby and E. F. Hasselbrink, Electrophoresis **25**, 187 (2004).
[26] D. Stein, M. Kruithof, and C. Dekker, Phys. Rev. Lett. **93**, 035901 (2004).
[27] C. Lee, L. Joly, A. Siria, A.-L. Biance, R. Fulcrand, and L. Bocquet, Nano Lett. **12** 4037 (2012).
[28] S. Kuga, J. Chromatogr. A **206**, 449 (1981).
[29] D. Vigolo, S. Buzzaccaro, and R. Piazza, Langmuir **26**, 7792 (2010).